Environmental Research Letters

LETTER

Benchmarking carbon fluxes of the ISIMIP2a biome models

Jinfeng Chang[1,2,16], Philippe Ciais[1], Xuhui Wang[1,3], Shilong Piao[3], Ghassem Asrar[4], Richard Betts[5], Frédéric Chevallier[1], Marie Dury[6], Louis François[6], Katja Frieler[7], Anselmo García Cantú Ros[7], Alexandra-Jane Henrot[6], Thomas Hickler[8,9], Akihiko Ito[10], Catherine Morfopoulos[5], Guy Munhoven[11], Kazuya Nishina[10], Sebastian Ostberg[7,12], Shufen Pan[13], Shushi Peng[3], Rashid Rafique[4], Christopher Reyer[7], Christian Rödenbeck[14], Sibyll Schaphoff[7], Jörg Steinkamp[8], Hanqin Tian[13], Nicolas Viovy[1], Jia Yang[13], Ning Zeng[15] and Fang Zhao[7]

1   Laboratoire des Sciences du Climat et de l'Environnement, UMR8212, CEA-CNRS-UVSQ, 91191 Gif-sur-Yvette, France
2   Sorbonne Universités (UPMC, Univ Paris 06)-CNRS-IRD-MNHN, LOCEAN/IPSL, 4 place Jussieu, 75005 Paris, France
3   Sino-French Institute of Earth System Sciences, College of Urban and Environmental Sciences, Peking University, 100871 Beijing People's Republic of China
4   Joint Global Change Research Institute, Pacific Northwest National Laboratory, College Park, Maryland, United States of America
5   College of Life and Environmental Sciences, University of Exeter, Exeter EX4 4QE, United Kingdom
6   Unité de Modélisation du climat et des Cycles Biogéochimiques, UR SPHERES, Université de Liège, Quartier Agora, Allée du Six Août 19 C, B-4000 Liège, Belgium
7   Potsdam Institute for Climate Impact Research, D-14412 Potsdam, Germany
8   Senckenberg Biodiversity and Climate Research Centre (BiK-F), Frankfurt am Main, Germany
9   Department of Physical Geography, Goethe-University, Frankfurt am Main, Germany
10 National Institute for Environmental Studies, Tsukuba, Ibaraki 305-8506, Japan
11 Laboratoire de Physique Atmosphérique et Planétaire, UR SPHERES, Université de Liège, Quartier Agora, Allée du Six Août 19 C, B-4000 Liège, Belgium
12 Geography Department, Humboldt-Universität zu Berlin, D-10099 Berlin, Germany
13 International Center for Climate and Global Change Research, School of Forestry and Wildlife Sciences, Auburn University, Auburn, AL, United States of America
14 Max Planck Institute for Biogeochemistry, Postfach 10 01 64, D-07701 Jena, Germany
15 Department of Atmospheric and Oceanic Sciences, University of Maryland, College Park, Maryland, United States of America
16 Author to whom any correspondence should be addressed.

E-mail: jinfeng.chang@locean-ipsl.upmc.fr

Abstract

The purpose of this study is to evaluate the eight ISIMIP2a biome models against independent estimates of long-term net carbon fluxes (i.e. Net Biome Productivity, NBP) over terrestrial ecosystems for the recent four decades (1971–2010). We evaluate modeled global NBP against 1) the updated global residual land sink (RLS) plus land use emissions (E_{LUC}) from the Global Carbon Project (GCP), presented as R + L in this study by Le Quéré *et al* (2015), and 2) the land CO_2 fluxes from two atmospheric inversion systems: Jena CarboScope s81_v3.8 and CAMS v15r2, referred to as F_{Jena} and F_{CAMS} respectively. The model ensemble-mean NBP (that includes seven models with land-use change) is higher than but within the uncertainty of R + L, while the simulated positive NBP trend over the last 30 yr is lower than that from R + L and from the two inversion systems. ISIMIP2a biome models well capture the interannual variation of global net terrestrial ecosystem carbon fluxes. Tropical NBP represents 31 ± 17% of global total NBP during the past decades, and the year-to-year variation of tropical NBP contributes most of the interannual variation of global NBP. According to the models, increasing Net Primary Productivity (NPP) was the main cause for the generally increasing NBP. Significant global NBP anomalies from the long-term mean between the two phases of El Niño Southern Oscillation (ENSO) events are simulated by all models ($p < 0.05$), which is consistent with the R + L estimate ($p = 0.06$), also mainly attributed to NPP anomalies, rather than to changes in heterotrophic respiration (Rh). The global NPP and NBP anomalies during ENSO events are dominated by their anomalies in tropical regions impacted by tropical climate variability. Multiple regressions between R + L, F_{Jena} and F_{CAMS} interannual variations and tropical climate

variations reveal a significant negative response of global net terrestrial ecosystem carbon fluxes to tropical mean annual temperature variation, and a non-significant response to tropical annual precipitation variation. According to the models, tropical precipitation is a more important driver, suggesting that some models do not capture the roles of precipitation and temperature changes adequately.

1. Introduction

Continuing and widespread environmental changes strongly impact the carbon cycling of terrestrial ecosystems, and thus land-atmosphere CO_2 fluxes. Terrestrial ecosystems have sequestrated 24%−33% of the anthropogenic carbon dioxide (CO_2) emissions in the last five decades (1965−2014; Le Quéré *et al* 2015), providing a negative feedback in the carbon-climate system (Friedlingstein *et al* 2006). Recent environmental changes have led to an increase in the global land carbon uptake. The global land carbon sink increased from 0.2 ± 0.5 Gt C yr^{-1} in 1960s to 2.1 ± 0.7 Gt C yr^{-1} in the last decade (2005−2014; Le Quéré *et al* 2015). The increasing net land carbon sequestration could be due to enhanced productivity caused by rising atmospheric CO_2 concentration (Cramer *et al* 2001, Smith *et al* 2016), nitrogen addition (including nitrogen fertilization and deposition), ecosystem management practices, and growing season extension in northern regions (e.g. Myneni *et al* 1997, Tucker *et al* 2001, Piao *et al* 2007). Here, the global net land carbon flux includes land-use-change emissions (E_{LUC}) and the 'residual' land sink (RLS) in the Global Carbon Project carbon budget from Le Quéré *et al* (2015). While data-driven assessments can only provide estimates of historical changes, it is essential to know how and to what extent the terrestrial carbon cycle will change in the future. In the past decades, global biome models have been developed to address these questions. Those models implement various processes to understand the global terrestrial carbon cycle, and have potential to project its future changes (e.g. Friedlingstein *et al* 2006, Sitch *et al* 2008). However, to increase the confidence in the associated future projections it is crucial to evaluate performance of the models.

The land CO_2 sink does not only show an increasing trend in the past five decades, but also an important interannual variability, of 1.2 Gt C yr^{-1} (standard deviation of the net land carbon flux in Le Quéré *et al* 2015) contributing to the observed fluctuations of the atmospheric carbon dioxide growth rate (CGR; Alden *et al* 2010, Baker *et al* 2006, Lee *et al* 1998, Le Quéré *et al* 2015). Therefore, besides evaluating model performances in estimating mean distribution and trends of terrestrial carbon fluxes, evaluation of the representation of interannual variability is also critical as it allows for testing our process understanding. The variation of terrestrial carbon fluxes is mainly influenced by climate, with

extreme climate events being generally associated with abnormal carbon sources in many observational case-studies of droughts and heat-waves (e.g. Zscheischler *et al* 2014a, 2014b at global scale; Wolf *et al* 2016 for U.S. drought in 2012; Ciais *et al* 2005 for Europe drought in 2003; and Gatti *et al* 2014 for Amazon drought in 2010). Climate anomalies (sometimes become extremes) cause a shift in the carbon balance of ecosystems mainly through their impacts on photosynthesis, respiration, fire occurrence and emissions, plants mortality and recruitment, insect outbreaks, and soil physical and biogeochemical changes (e.g. erosion, carbon, nutrients, etc.) (Reichstein *et al* 2013, Frank *et al* 2015). These disturbances by climate anomalies generally reduce the terrestrial carbon sink or cause net carbon sources from terrestrial ecosystems during a few months, but can lead to recovery sinks in the following years.

At global scale, the El Niño Southern Oscillation (ENSO) is the largest-known global mode of interannual climate variability (Dawson and O'Hare, 2000). The ENSO-driven fluctuations of carbon fluxes over tropical land areas play the most important role in explaining global CGR and carbon flux variations. Therefore, a specific focus in this study is the evaluation of modeled global and tropical carbon flux anomalies during ENSO events.

We present a global evaluation of the eight ISIMIP2a biome models for their ability to capture (1) the current mean value and historical trends of the net land carbon flux, (2) carbon flux anomalies during ENSO events, and (3) the sensitivity of carbon fluxes to tropical climate variability.

2. Material and methods

2.1. ISIMIP2a biome models and the simulation protocol

The models involved in ISIMIP2a biome sector simulations are: CARAIB (Warnant *et al* 1994, Gérard *et al* 1999, Dury *et al* 2011), DLEM (Tian *et al* 2015a), JULES (Best *et al* 2011, Clark *et al* 2011), LPJ-GUESS (Smith *et al* 2014), LPJmL (Bondeau *et al* 2007), ORCHIDEE (Krinner *et al* 2005), VEGAS (Zeng *et al* 2005), and VISIT (Ito and Inatomi 2012). All models simulated the carbon cycles of terrestrial ecosystem in response to climate change and rising atmospheric CO_2 concentration, with varying degree of detailed representation of vegetation types.

The same climate forcing (two different datasets at daily time step and at a spatial resolution of $0.5° \times 0.5°$) and global atmospheric CO_2 concentration (Keeling and Whorf 2005, data continue to be updated) data were used by all models. Historical land-use data provided by ISIMIP2a see text S1 stacks.iop.org/ERL/12/045002/mmedia of supplementary material for detail) were used by 7 models, CARAIB being the exception because its simulations did not prescribed land-use (i.e. run with potential natural vegetation). The ISIMIP2a climate forcing data differs from TRENDY (Sitch *et al* 2015) and MsTMIP (Huntzinger *et al* 2013), since these experiments used only CRU-NCEP data (Viovy 2014). From the ISIMIP2a runs, we used all simulations forced by two reconstructed historical climate forcing datasets, namely the Princeton Global Meteorological Forcing Dataset (PGFv2; http://hydrology.princeton.edu/data.pgf.php) and GSWP3 (http://hydro.iis.u-tokyo.ac.jp/GSWP3) with time spans of 1901–2012, 1901–2010 respectively. In total 16 simulations (8 models × 2 climate forcing datasets) were used in this study. According to the simulation protocol (www.isimip.org/gettingstarted/#simulation-protocol), each simulation comprised of (i) a 'spin-up' run to equilibrate the vegetation and soil carbon pools using cycled climate forcing of early decades of the 20th century (e.g. 1901–1930), pre-industrial CO_2 concentration, and land-use status before the beginning of 20th century; and (ii) followed by a 'transient' run since 1901 forced by historical climate, CO_2 concentration and land-use change. The model outputs for the period 1971–2010 were used in this study. Two models, DLEM and LPJ-GUESS, included Carbon-Nitrogen interaction, thus were able to respond to time variable nitrogen deposition (for DLEM: Wei *et al* 2014, Tian *et al* 2015b, for LPJ-GUESS: Lamarque *et al* 2011, 2013), nitrogen fixation (for LPJ-GUESS only: Cleveland *et al* 1999), and nitrogen fertilization (for DLEM only: Lu and Tian 2017).

2.2. The global NBP and component fluxes
NBP represents the net carbon flux between terrestrial ecosystem and atmosphere, and is calculated as:

$$NBP = NEP - C_{harvest} - C_{fire} \qquad (1)$$

where $C_{harvest}$ is carbon exported from ecosystems as harvested biomass and/or forest products; C_{fire} is the carbon lost due to fire emissions; NEP is net ecosystem productivity calculated by the difference between NPP and Rh:

$$NEP = NPP - Rh. \qquad (2)$$

It should be noted that some models did not include all the above elements of NBP: $C_{harvest}$ was not simulated by CARAIB, JULES, and LPJ-GUESS, and C_{fire} was not considered in DLEM, JULES, and ORCHIDEE. For models accounting for forest harvest (i.e. VEGAS and VISIT), the harvested wood is allocated to pools with different decay rates (e.g. 1 yr, 10 yr and 100 yr for VISIT) to calculate $C_{harvest}$ from forest products. The key model processes impacting NBP components are described in table S1.

To our knowledge, there is no direct global observation of the land carbon balance (i.e. NBP in biome models' simulations), except for the global forest sink on decadal scale (Pan *et al* 2011). Due to the varying degree of detail in the representation of vegetation types among models, the forest carbon balance dataset cannot be used to benchmark modeled NBP. The GCP carbon budget reported by Le Quéré *et al* (2015) provided an estimate of the land carbon balance decomposed into two components: net land-use change emissions (E_{LUC}) and the 'residual' land sink (RLS; see Text S2 of supplementary material for detail information on E_{LUC} and RLS). Given that land-use change was taken into account in most ISIMIP2a biome model simulations, the simulated gridded NBP from them was aggregated to a global mean to be comparable to the sum of RLS and E_{LUC} (hereafter referred to as R + L).

2.3. Materials used in the benchmarking analysis
In this study, several materials other than R + L were used in the benchmarking analysis (section 2.4). They are (1) the Multivariate ENSO Index (MEI) used to define 'moderate to strong' ENSO events (Wolter and Timlin 2011); (2) the NOAA/AVHRR composite GIMMS-NDVI data (Tucker *et al* 2005); and (3) the total land fluxes from two inversion systems: the Jena CarboScope s81_v3.8 (Rödenbeck *et al* 2003, 2006; hereafter referred to as F_{Jena}), and CAMS v15r2 (Chevallier *et al* 2005, 2010, Chevallier 2013, hereafter referred to as F_{CAMS}). The detail descriptions of these materials were presented in the Text S3 to S5 of supplementary material. In this study, we focused on carbon fluxes over vegetated land, defined as the land grid cells with mean NDVI larger than 0.1 over the period 1982–2010.

2.4. Benchmarking analysis
2.4.1. Carbon flux changes during ENSO events
To evaluate modeled carbon fluxes anomalies in ENSO events, we separated modeled NBP detrended anomalies (hereafter referred to as NBP^{var}, where the detrended anomaly, i.e. the interannual variability is indicated by the 'var' superscript) and R + L detrended anomalies (R + L^{var}) during El Niño and La Niña years (section 2.3). A two-tailed Student's t-test with a 0.05 significance level was used to detect the carbon flux deviations between the two phases of ENSO events. Furthermore, the spatial pattern of NBP^{var} in ENSO events was compared to that of NDVI detrended anomalies (NDVI^{var}) to test the hypothesis that above-ground biomass/productivity dynamics may drive the NBP negative (source anomaly). To generate a model-dependent but forcing-independent response, the anomalies from the model output driven by the two climate forcings were used for each biome model (i.e. 80 anomalies for each model, 40 yr per forcing × 2 climate forcings).

Figure 1. The magnitude of global GPP and NBP estimated by the eight ISIMIP2a biome models driven by the two climate forcing datasets respectively. *x*-axis indicates mean annual global GPP during 1971–2010 with error bars showing standard deviation of the interannual variations. *y*-axis indicates mean annual global NBP during 1971–2010 with error bars showing standard deviation of the interannual variations. The black line shows global Residual Land Sink (RLS) plus land use change emissions (ELUC) (R + L; Le Quéré *et al* 2015).

2.4.2. Response of carbon fluxes to tropical climate variations

We used a multiple regression approach to diagnose, from the model simulations, the response of carbon flux (Gross primary productivity (GPP) or NBP) to tropical climate variability over the period 1981−2010:

$$y^{\mathrm{var}} = \gamma^{\mathrm{int}} \times T^{\mathrm{var}} + \delta^{\mathrm{int}} \times P^{\mathrm{var}} + \varphi^{\mathrm{int}} \times \mathrm{SW}^{\mathrm{var}} + \varepsilon \qquad (3)$$

where y is a global carbon flux (i.e. GPP, NBP, F_{Jena}, F_{CAMS}, or R + L); T is the tropical mean annual temperature; P is the tropical annual precipitation; SW is the tropical downward short-wave radiation. The tropical climate values were calculated as the spatial average over vegetated tropical lands (23°N to 23°S) with mean NDVI larger than 0.1 for the period 1982–2010 The fitted regression coefficients γ^{int}, δ^{int}, and φ^{int} are *apparent carbon flux* (GPP, NBP, F_{Jena}, F_{CAMS}, or R + L) *sensitivities* as defined in Piao *et al* (2013) to interannual variations in tropical mean annual temperature, annual precipitation and solar radiation respectively, and ε the residual error term. As emphasized in Piao *et al* (2013), γ^{int}, δ^{int}, and φ^{int} are not the 'true' sensitivities of carbon fluxes because of (i) temperature, precipitation and solar radiation all covary over time; and (ii) other climate drivers discarded in equation (3), such as humidity, and wind speed may also contribute to the variability of carbon fluxes. The regression coefficients are maximum likelihood estimates. The uncertainty in γ^{int}, δ^{int}, and φ^{int} was represented as the standard error of the corresponding regression coefficients. To generate a model-dependent but forcing-independent response, the anomalies from the model output driven by the two

climate forcings were combined for each regression (i.e. for each model, 80 anomalies, 40 yr per forcing × 2 climate forcings, of model output and the corresponding climate anomalies were used). We have excluded the years that immediately follow major volcanic eruptions (i.e. El Chichón, Mexico: 1982−1983; and Pinatubo, Philippine: 1991−1993), since during these years the carbon cycle may have been significantly perturbed by changes in radiation quantity and diffuse fraction (Robock 2000) that were not included in our climate forcing datasets.

For regression of $F_{\mathrm{Jena}}^{\mathrm{var}}$, $F_{\mathrm{CAMS}}^{\mathrm{var}}$, and data-based R + L$^{\mathrm{var}}$, we used mean annual temperature data from the Climatic Research Unit (CRU) at the University of East Anglia (Mitchell and Jones 2005), precipitation data from CRU and GPCC, solar radiation from CRU-NCEP v4 dataset (http://dods.extra.cea.fr/data/p529viov/cruncep/), which were the same as the datasets used by Piao *et al* (2013).

3. Results

3.1. NBP estimation and comparison with observation

There are large differences among the modeled NBP (that includes 7 models with land-use change) over the period 1971–2010, ranging from 0.3 Pg C yr^{-1} (LPJmL-PGFv2) to 2.6 Pg C yr^{-1} (VISIT-GSWP3) with a year-to-year variability ranging from 0.6 Pg C yr^{-1} (DLEM-PGFv2) to 1.6 Pg C yr^{-1} (LPJ-GUESS-GSWP3). The model ensemble-mean NBP is 1.3 Pg C yr^{-1} and 1.4 Pg C yr^{-1} driven by PGFv2 and GSWP3 forcings respectively, which is higher than the R + L

Figure 2. The magnitude of the global NBP trend over 1971–2010 estimated by the model-forcing simulation ensemble, and the correlation coefficient between modeled NBP interannual variability and interannual variability in global Residual Land Sink (RLS) plus land use change emissions (ELUC) (R + L; Le Quéré *et al* 2015). Dashed line indicates the trend derived from R + L (Le Quéré *et al* 2015).

(mean value of 0.8 Pg C yr^{-1} with a year-to-year variability of 1.2 Pg C yr^{-1}). Positive NBP trends are found from all 14 simulations that considered land-use change during the period of 1971–2010 (0.015 ± 0.010 Pg C yr^{-2}; figure 2), while larger positive trends are obtained for the period 1981–2010 (0.041 ± 0.016 Pg C yr^{-2}; table 1). However, the model ensemble-mean NBP trend from ISIMIP2a models was lower than the trends estimated from R + L and the two inversion systems during the same period (table 1). For the analysis of the interannual variability in modeled NBP, the models generally show good agreement between the NBP variability and the variability of R + L ($r = 0.6 \pm 0.1$, with all correlation significant at $p < 0.05$ for the period 1971–2010; figure 2), and that of the land sink from both atmospheric inversions ($r = 0.6 \pm 0.1$ and $r = 0.6 \pm 0.1$, with all correlation significant at $p < 0.05$ for the period 1981–2010 for Jena CarboScope s81_v3.8 and for CAMS v15r2 respectively). The interannual variation of R + L and the land carbon flux from the two atmospheric inversions are very similar ($r > 0.9$ for any two of the dataset).

Model ensemble-mean NBP from tropical (23°S–23°N), North Hemisphere extra-tropical (NH extra-tropical: 23°N–90°N), and South Hemisphere extra-tropical (SH extra-tropical: 90°S–23°S) ecosystems represent $31 \pm 17\%$, $64 \pm 19\%$ and $5 \pm 4\%$ of global NBP respectively for the period of 1971–2010, across all ISIMIP2a models. The year-to-year variations of tropical NBP are 0.9 ± 0.3 Pg C yr^{-1} (table 2), which is much higher than that of NBP in NH (0.4 ± 0.2 Pg C yr^{-1}) and SH extra-tropical ecosystems (0.2 ± 0.1 Pg C yr^{-1}). The correlation (r) between the interannual variation of global NBP and tropical NBP reaches 0.90 ± 0.05, which is higher than that between the interannual variation of global NBP and extra-tropical NBP ($r = 0.3 \pm 0.2$ between NH extra-tropical and global NBP; $r = 0.5 \pm 0.2$ between SH extra-tropical and global NBP).

More than 85% (i.e. 12 out of 14) of simulations considering land-use change agree on the existence of significant carbon sink over 42% of vegetated land (i.e. 47×10^6 km^2), including strong carbon sinks (positive NBP larger than 20 gC $m^{-2}yr^{-1}$) for intact tropical forest regions (in South America, Africa and Southeast Asia), eastern United States, south China, southeast Asia, as well as weak carbon sinks in high latitudes and northeast Australia (figure 3(*a*); figure S1). A negative ensemble-mean NBP (carbon source) is simulated in fewer regions, namely southeast South America, Sub-Saharan Africa, and Middle East. However, these negative NBP regions, covering 23×10^6 km^2, are not consistent in the different simulations. Significant negative NBP (i.e. a net CO_2 source) is only consistent across most models ($> 85\%$ of simulations) over 1.4×10^6 km^2 (i.e. only 1.3% of vegetated land; figure 3(*a*); figure S1). The model ensemble-mean trend of NBP shows distinct spatial patterns. A significant decrease of NBP is simulated with a good agreement between most models ($> 85\%$ of simulations) over 8.1×10^6 km^2 of land, concentrated over South America (including the Amazon forest), western North America, southeastern Africa, northeastern India, southeast Asia, northeastern China, and some grid cells in central Australia (figure 3(*b*). The NBP positive trends simulated across most models ($> 85\%$ of simulations) are significant and in close agreement over 20.6×10^6 km^2 of vegetated land (e.g. Alaska, northeastern North America, high-latitude Eurasia, sub-Saharan western Africa, Angola, and southern China).

Table 1. Mean NBP and NBP trend estimation from ISIMIP2a models, R + L, inversions and TRENDY models, and the correlation of NBP interannual variability among them. Values for different periods are shown depending on the time span of datasets used to compare. The ensemble-mean NBP and its trend from ISIMIP2a models account for 7 models with land-use change (i.e. excluding CARAIB), while the correlation on interannual variability account for all 8 ISIMIP2a models.

		ISIMIP2a		R + L (Le Quéré *et al* 2015)	Inversions		TRENDY (Sitch *et al* 2015)
	Period	PGFv2	GSWP3		Jena CarboScope s81_v3.8	CAMS v15r2	
Mean NBP ($Pg\,C\,yr^{-1}$)	1971−2010	1.32 ± 0.76 (Var. 0.99 ± 0.33)	1.44 ± 0.77 (Var. 1.08 ± 0.36)	0.79 ± 1.16			
	1981−2010	1.34 ± 0.78 (Var. 0.96 ± 0.35)	1.41 ± 0.76 (Var. 1.08 ± 0.38)	0.94 ± 1.21	0.90 ± 1.05	1.80 ± 1.24	
	1990–2009	1.51 ± 0.75 (Var. 0.85 ± 0.34)	1.49 ± 0.76 (Var. 1.03 ± 0.41)	1.24 ± 1.14	1.23 ± 0.95	2.22 ± 1.06	2.38 ± 0.72[b]
Trend ($Pg\,C\,yr^{-2}$)	1971–2010	0.019 ± 0.010	0.010 ± 0.010	0.036			
	1981–2010	0.044 ± 0.020	0.038 ± 0.013	0.052[a]	0.065[a]	0.085[a]	
	1990–2009	0.044 ± 0.022	0.060 ± 0.024	0.026	0.052	0.057	0.055 ± 0.030
Correlation on Interannual variability (unitless)	1971–2010 vs. R + L	0.61 ± 0.08[a]	0.65 ± 0.07[a]				
	1981–2010 vs. R+L	0.59 ± 0.10[a]	0.64 ± 0.08[a]				
	vs. Jena CarboScope s81_v3.8	0.64 ± 0.12[a]	0.65 ± 0.09[a]				
	vs. CAMS v15r2	0.58 ± 0.15[a]	0.61 ± 0.10[a]				

[a] Indicates the NBP trend is significant with $p < 0.05$.
[b] Ensemble-mean NBP from TRENDY did not consider land-use change.
Var. in ensemble-mean NBP from ISIMIP2a models indicates the ensemble-mean year-to-year variation ± the standard deviation among models.
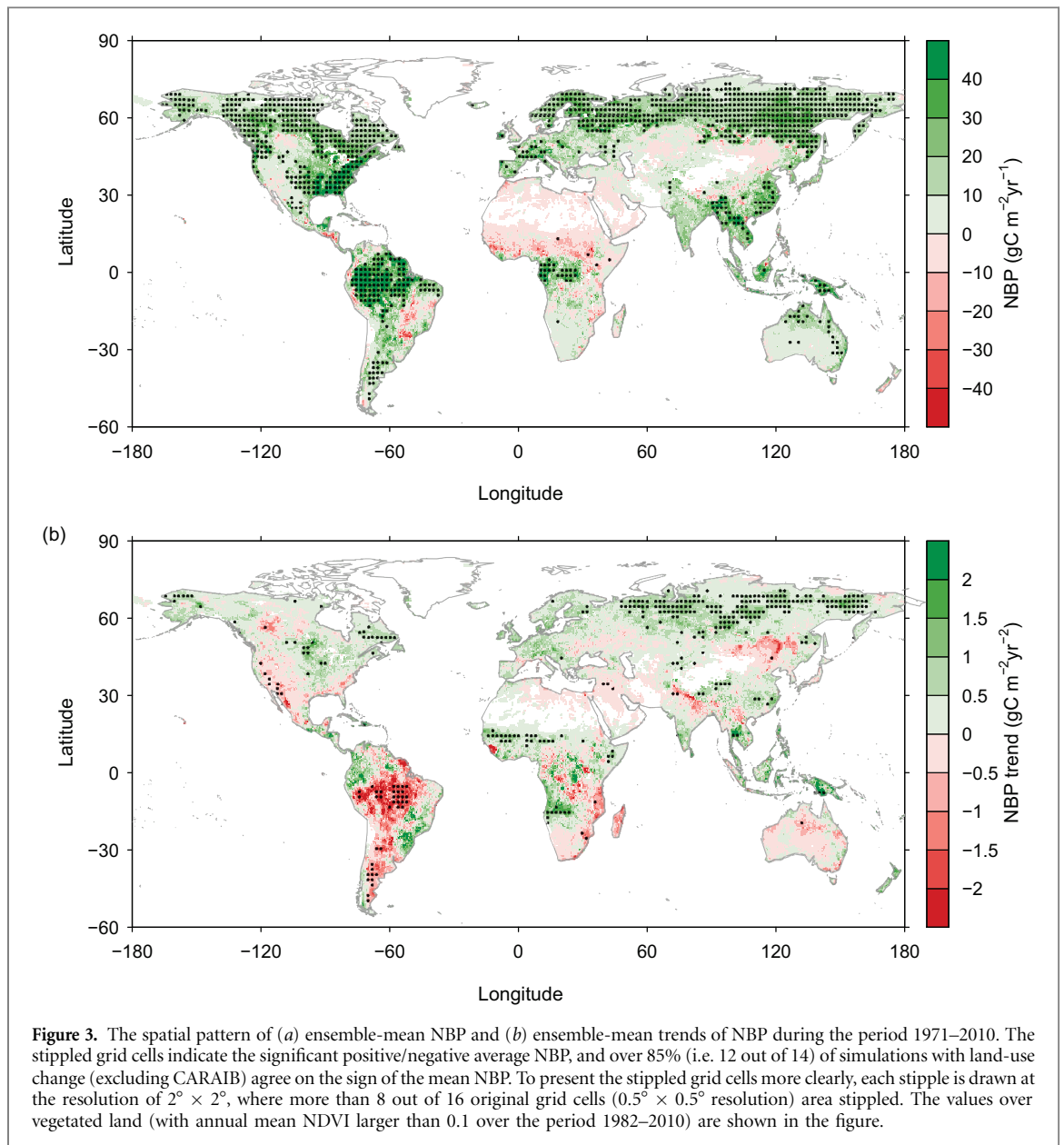
Table 2. The interannual variability of NBP, NPP and Rh, and their anomalies in years with significantly negative and positive model ensemble-mean global NBP anomaly respectively. The interannual variability and the anomalies are shown over the whole globe, tropical region, and extra-tropical region respectively. We further divided tropical region into tropical forest and non-forest regions according to the MODIS MCD12C1 land cover type classification. Tropical forest is defined as the grid cells with dominant forest land cover type (i.e. forest cover is more than 50% of land).

	Interannual variation expressed as the standard deviation of detrended time series					
	Global	NH extra-tropical	SH extra-tropical	Tropical	Tropical forest	Tropical non-forest
NBP ($Pg\,C\,yr^{-1}$)	1.05 ± 0.34	0.37 ± 0.17	0.23 ± 0.12	0.89 ± 0.30	0.47 ± 018	0.52 ± 0.20
NPP ($Pg\,C\,yr^{-1}$)	1.05 ± 0.21	0.43 ± 0.08	0.26 ± 0.08	0.86 ± 0.24	0.41 ± 0.16	0.58 ± 0.16
Rh ($Pg\,C\,yr^{-1}$)	0.52 ± 0.13	0.31 ± 0.08	0.11 ± 0.04	0.33 ± 0.15	0.17 ± 0.11	0.24 ± 0.09
	Positive global NBP anomaly years					
NBP ($Pg\,C\,yr^{-1}$)	0.66 ± 0.26	0.05 ± 0.06	0.09 ± 0.06	0.52 ± 0.18	0.24 ± 0.10	0.28 ± 0.10
NPP ($Pg\,C\,yr^{-1}$)	0.60 ± 0.20	−0.01 ± 0.07	0.10 ± 0.05	0.51 ± 0.15	0.22 ± 0.10	0.29 ± 0.08
Rh ($Pg\,C\,yr^{-1}$)	−0.02 ± 0.12	−0.05 ± 0.03	0.01 ± 0.03	0.02 ± 0.10	−0.00 ± 0.07	0.03 ± 0.05
	Negative global NBP anomaly years					
NBP ($Pg\,C\,yr^{-1}$)	−0.58 ± 0.26	0.02 ± 0.09	−0.10 ± 0.07	−0.50 ± 0.17	−0.26 ± 0.11	−0.24 ± 0.10
NPP ($Pg\,C\,yr^{-1}$)	−0.53 ± 0.25	0.09 ± 0.10	−0.12 ± 0.05	−0.49 ± 0.17	−0.24 ± 0.11	−0.26 ± 0.10
Rh ($Pg\,C\,yr^{-1}$)	0.02 ± 0.15	0.07 ± 0.05	−0.03 ± 0.04	−0.02 ± 0.10	0.00 ± 0.05	−0.02 ± 0.05

3.2. NBP anomalies during ENSO events

The simulated NBP by all models are significantly ($p < 0.05$) larger (stronger carbon sink or weaker carbon source) during La Niña years than that during El Niño years, consistent with the data-based R + L (even though only significant at $p = 0.06$; figure 4). The modeled global composite NBP anomaly difference between the two phases of ENSO events (hereafter $\Delta NBP_{L-E} = NBP_{LaNiña} - NBP_{ElNiño}$) is

$1.5 \pm 0.5\,Pg\,C\,yr^{-1}$, which is larger than that estimated from R + L ($1.0\,Pg\,C\,yr^{-1}$). This NBP difference is in the models mainly due to the NPP differences (hereafter $\Delta NPP_{L-E} = NPP_{LaNiña} - NPP_{ElNiño}$, of $1.6 \pm 0.4\,Pg\,C\,yr^{-1}$, i.e. $3.0 \pm 0.8\%$ of modeled global mean annual NPP) rather than being the result of Rh differences ($\Delta Rh_{L-E} = Rh_{LaNiña} - Rh_{ElNiño}$, 0.3 ± 0.4 $Pg\,C\,yr^{-1}$, i.e. $0.6 \pm 0.8\%$ of modeled global mean annual Rh). It is noteworthy that positive ΔRh_{L-E}

Figure 3. The spatial pattern of (*a*) ensemble-mean NBP and (*b*) ensemble-mean trends of NBP during the period 1971–2010. The stippled grid cells indicate the significant positive/negative average NBP, and over 85% (i.e. 12 out of 14) of simulations with land-use change (excluding CARAIB) agree on the sign of the mean NBP. To present the stippled grid cells more clearly, each stipple is drawn at the resolution of 2° × 2°, where more than 8 out of 16 original grid cells (0.5° × 0.5° resolution) area stippled. The values over vegetated land (with annual mean NDVI larger than 0.1 over the period 1982–2010) are shown in the figure.
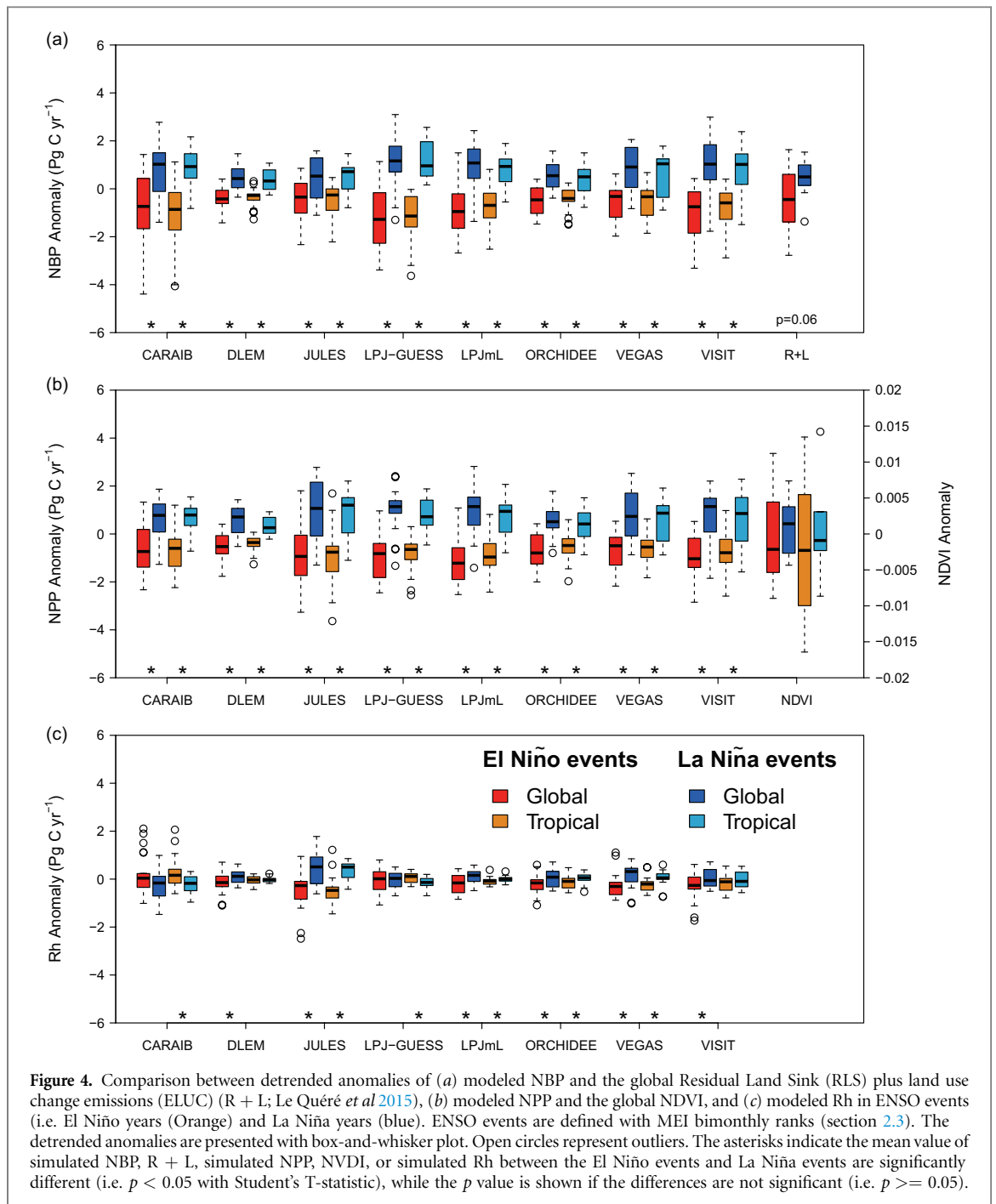
are simulated by 6 out of 8 models, and negative ΔRh_{L-E} are simulated by CARAIB and LPJ-GUESS. The residual ΔNBP_{L-E} can be attributed to anomalies of C_{fire} or $C_{harvest}$ (equations (1) and (2)) caused by the ENSO events. These processes are only taken into account in some models (section 2.2), which precludes a more systematic analysis. NDVI data also shows a higher mean value during La Niña years than that during El Niño years ($\Delta NDVI_{L-E} = 0.0017$, i.e. 0.4% of global mean annual NDVI), whereby the difference is not significant ($p = 0.53$). It is also noteworthy that the ΔNBP_{L-E} and ΔNPP_{L-E} over tropical region (23°S−23°N) are 1.4 ± 0.6 Pg C yr^{-1} and 1.3 ± 0.4 Pg C yr^{-1} respectively, and contributed to most of the modeled global NBP and NPP differences between La Niña and El Niño events (figures 4(*a*) and (*b*)).

During El Niño years, strong negative NBP anomalies (<-20 g C m^{-2} yr^{-1}) are simulated in most tropical and sub-tropical regions (30°S−30°N) except in southern Brazil and eastern Africa, while positive NBP anomalies during El Niño years are simulated in western temperate North America, southern Brazil, and in some regions of temperate and boreal central Asia (figure 5). During La Niña years, in general opposite NBP anomaly patterns are simulated. More than 87.5% of the simulations (i.e. 14 out of 16) agree well on the sign (negative/positive) of NBP/NPP anomalies in regions where strong mean anomalies are simulated (figure 5).

The spatial patterns of simulated mean NPP anomalies during both phases of ENSO (figures 5(*c*) and (*d*)) are very similar to those of mean NBP anomalies (figures 5(*a*) and (*b*)). Generally, the simulated NPP mean anomalies during both phases of ENSO are similar to observed NDVI anomalies. Significant NPP anomalies (negative and positive) are consistently simulated by 14 out of 16 simulations over 39% (i.e. 44×10^6 km^2) and 40% (i.e. 46×10^6 km^2) of vegetated land during El Niño years and during La Niña years respectively. Within those areas with

Figure 4. Comparison between detrended anomalies of (*a*) modeled NBP and the global Residual Land Sink (RLS) plus land use change emissions (ELUC) (R + L; Le Quéré *et al* 2015), (*b*) modeled NPP and the global NDVI, and (*c*) modeled Rh in ENSO events (i.e. El Niño years (Orange) and La Niña years (blue). ENSO events are defined with MEI bimonthly ranks (section 2.3). The detrended anomalies are presented with box-and-whisker plot. Open circles represent outliers. The asterisks indicate the mean value of simulated NBP, R + L, simulated NPP, NVDI, or simulated Rh between the El Niño events and La Niña events are significantly different (i.e. $p < 0.05$ with Student's T-statistic), while the p value is shown if the differences are not significant (i.e. $p >= 0.05$).
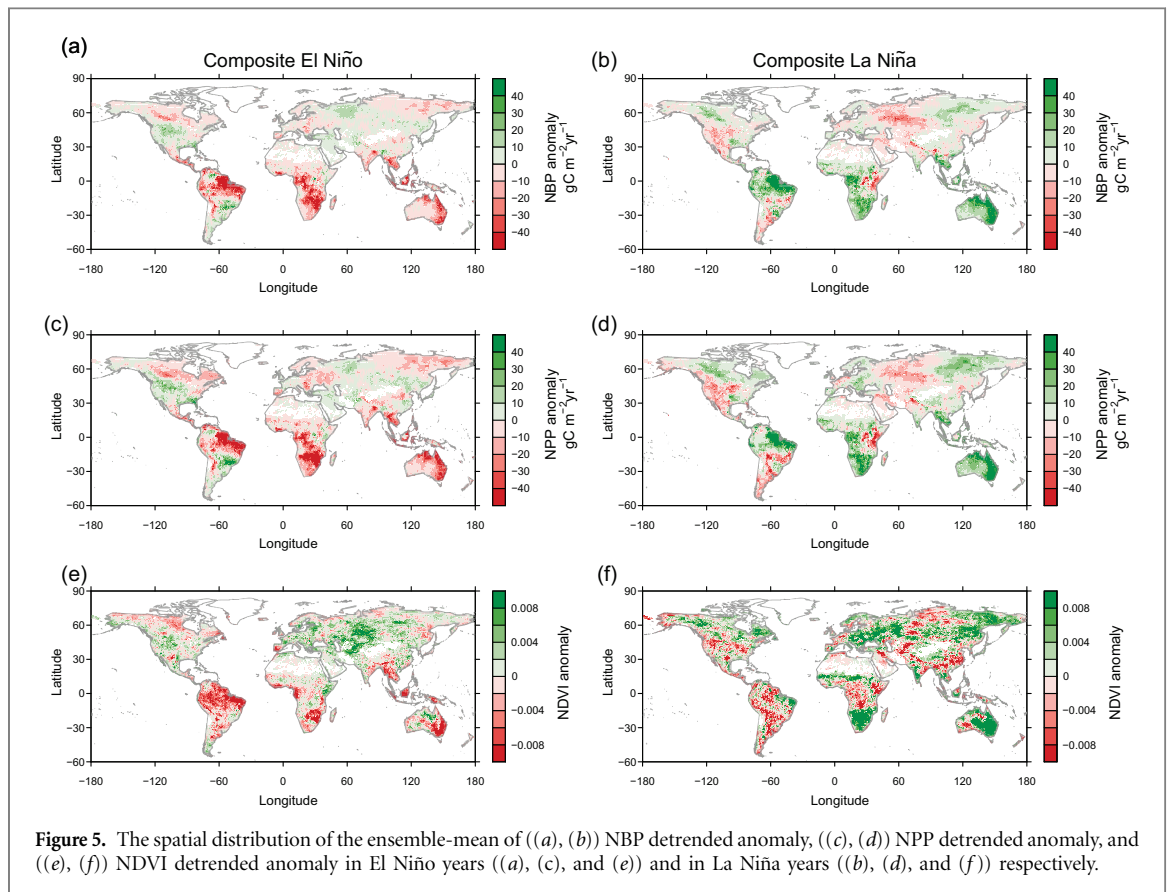
significant NPP anomalies represented by over 87.5% of the simulations, observed NDVI anomalies are of the same sign as model ensemble-mean NPP anomalies for 72% and 69% of the area during El Niño years and La Niña years respectively. However, negative NDVI anomalies during the La Niña years are observed in the lower part of the Amazon basin and tropical forest in Africa, where positive NPP anomalies are simulated.

3.3. Variation of global GPP and NBP coupled with tropical temperature, precipitation and solar radiation variability

The interannual variation of modeled global GPP is significantly and negatively correlated with tropical temperature variation in 2 out of 8 models (JULES and VISIT; all time series are detrended), but the magnitude of the responses is largely different and even the sign of γ_{GPP}^{int} can be different among models (e.g. positive interannual correlation is found for DLEM; figure 6(*a*)). The GPP interannual sensitivity to tropical precipitation variation is always positive, resulting in a mean sensitivity of 1.0 ± 0.4 Pg C yr^{-1} per 100 mm (response is significant at level $p < 0.05$ for the 4 out of 8 models; figure 6(*b*)). The correlation between modeled GPP variation and tropical solar radiation variation is insignificant for all models (figure 6(*c*)).

In contrast to the response of global GPP to tropical temperature, significantly negative responses

Figure 5. The spatial distribution of the ensemble-mean of ((*a*), (*b*)) NBP detrended anomaly, ((*c*), (*d*)) NPP detrended anomaly, and ((*e*), (*f*)) NDVI detrended anomaly in El Niño years ((*a*), (*c*), and (*e*)) and in La Niña years ((*b*), (*d*), and (*f*)) respectively.
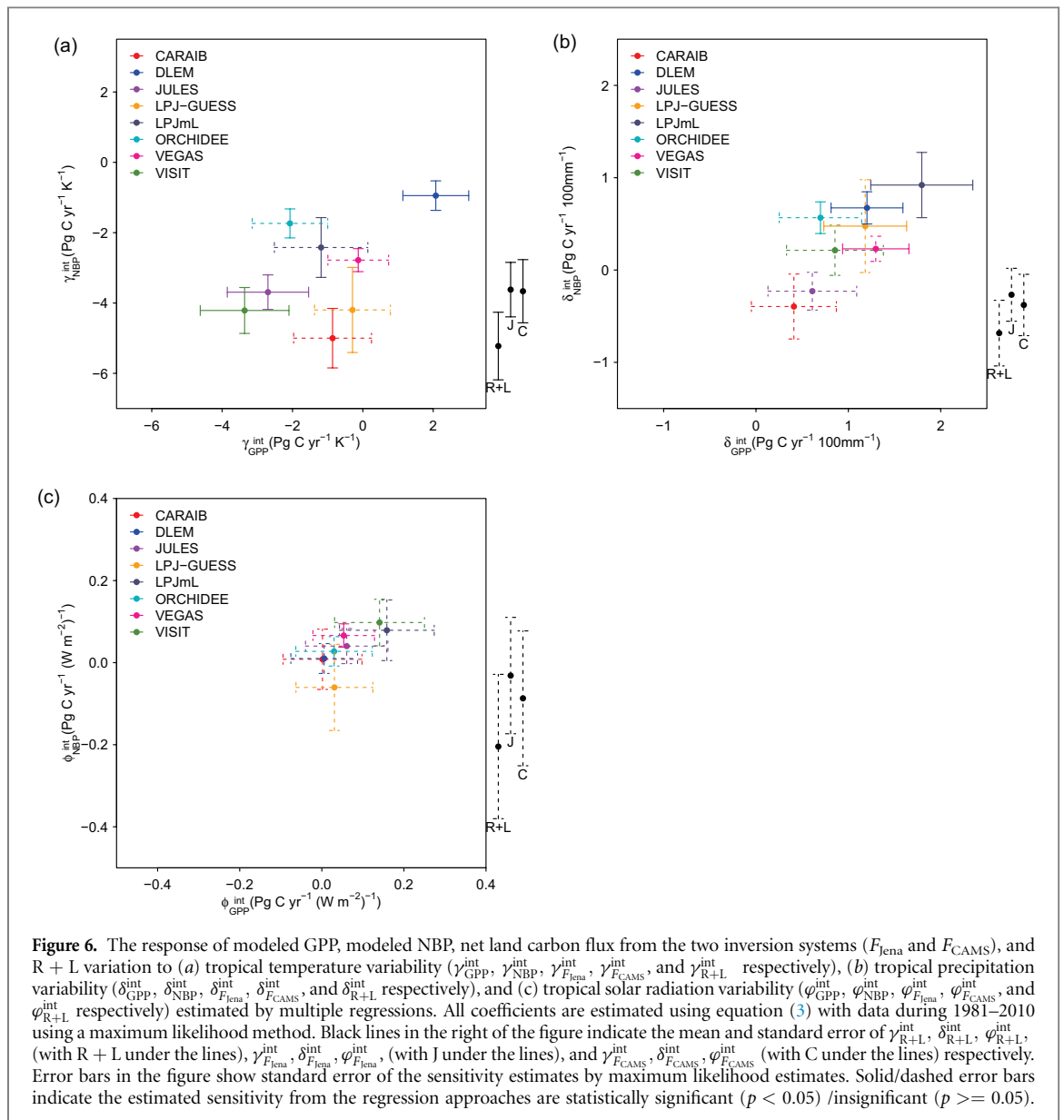
of modeled NBP variation to tropical temperature variation are found in all ISIMIP2a biome models, i.e. reduced uptake or larger sources (-3.1 ± 1.4 Pg C yr^{-1} K^{-1}, all $p < 0.05$). $\gamma_{\text{NBP}}^{\text{int}}$ ranges from -1.0 ± 0.4 Pg C yr^{-1} K^{-1} for DLEM to -5.0 ± 0.8 Pg C yr^{-1} K^{-1} for CARAIB (figure 6(*a*)). The *apparent* R+ L *sensitivity* to tropical temperature variation ($\gamma_{\text{R+L}}^{\text{int}} = -5.2 \pm 1.0$ Pg C yr^{-1}K^{-1}, $p < 0.01$) is larger than all, $\gamma_{\text{NBP}}^{\text{int}}$, $\gamma_{F_{\text{Jena}}}^{\text{int}}$ (-3.6 ± 0.8 Pg C yr^{-1} K^{-1}, $p < 0.01$) and $\gamma_{F_{\text{CAMS}}}^{\text{int}}$ (-3.7 ± 0.9 Pg C yr^{-1} K^{-1}, $p < 0.01$). The F_{Jena}, F_{CAMS}, data-based R + L is not significantly correlated with tropical precipitation variation (negative correlations), while modeled NBP variation shows significantly positive response to tropical precipitation variation in 3 out of 8 models (DLEM, LPJmL and ORCHIDEE; figure 6(*b*)). Similar to $\varphi_{\text{GPP}}^{\text{int}}$, no significant $\varphi_{\text{NBP}}^{\text{int}}$ is found for the *apparent* NBP *sensitivity* to tropical solar radiation variation among models, and the results are the same for $\varphi_{\text{R + L}}^{\text{int}}$, $\varphi_{F_{\text{Jena}}}^{\text{int}}$ and $\varphi_{F_{\text{CAMS}}}^{\text{int}}$ (figure 6(*c*)).

4. Discussion

4.1. Net carbon fluxes of the ISIMIP2a biome models
The model ensemble-mean NBP (across the 7 models with land-use change) is higher than, but within the uncertainty of R + L for the period 1971–2010 (figure 1), indicating that the models overestimate the observed terrestrial net carbon flux. The reasons could

include but are not limited to inadequate representation of some processes leading to carbon loss from ecosystems in the models. For example, crop harvest is not taken into account in JULES and LPJ-GUESS; fire emissions are not included in DLEM, JULES and ORCHIDEE; wood harvest is only considered in VEGAS and VISIT. However, NBPs from models that include those 3 processes (i.e. VEGAS and VISIT; with NBP of 1.7 ± 0.9 Pg C yr^{-1}) do not show a better agreement with R + L. In addition, shifting cultivation is not considered in all simulations, which could bring uncertainties on the modeled land-use emission (e.g. Stocker *et al* 2014). The model ensemble-mean NBP from ISIMIP2a models is between the independent model ensemble-mean NBP from TRENDY (1.0 ± 0.4 Pg C yr^{-1} with year-to-year variation of 1.0 ± 0.2 Pg C yr^{-1}, including Land-Use Change Emissions and Terrestrial Sink simulated by TRENDY models) and MsTMIP (1.5 ± 1.4 Pg C yr^{-1} with year-to-year variation of 0.5 ± 0.1 Pg C yr^{-1}; derived from SG3 runs with changing CO_2, climate, and land-use; Huntzinger *et al* 2013) for the same period (1971–2010). The difference could come from the different models participating in ISIMIP2a (although some common models such as ORCHIDEE and VISIT participated in all projects), from the different model versions, as well as from the climate forcings (e.g. CRU-NCEP for TRENDY and MsTMIP) and/or land-use/land-cover changes forcings (e.g. prescribed in MsTMIP). For example, large differences in simulated NBP are found in common models (but different model version) driven

Figure 6. The response of modeled GPP, modeled NBP, net land carbon flux from the two inversion systems (F_{Jena} and F_{CAMS}), and R + L variation to (*a*) tropical temperature variability (γ_{GPP}^{int}, γ_{NBP}^{int}, $\gamma_{F_{Jena}}^{int}$, $\gamma_{F_{CAMS}}^{int}$, and γ_{R+L}^{int} respectively), (*b*) tropical precipitation variability (δ_{GPP}^{int}, δ_{NBP}^{int}, $\delta_{F_{Jena}}^{int}$, $\delta_{F_{CAMS}}^{int}$, and δ_{R+L}^{int} respectively), and (*c*) tropical solar radiation variability (φ_{GPP}^{int}, φ_{NBP}^{int}, $\varphi_{F_{Jena}}^{int}$, $\varphi_{F_{CAMS}}^{int}$, and φ_{R+L}^{int} respectively) estimated by multiple regressions. All coefficients are estimated using equation (3) with data during 1981–2010 using a maximum likelihood method. Black lines in the right of the figure indicate the mean and standard error of γ_{R+L}^{int}, δ_{R+L}^{int}, φ_{R+L}^{int}, (with R + L under the lines), $\gamma_{F_{Jena}}^{int}$, $\delta_{F_{Jena}}^{int}$, $\varphi_{F_{Jena}}^{int}$, (with J under the lines), and $\gamma_{F_{CAMS}}^{int}$, $\delta_{F_{CAMS}}^{int}$, $\varphi_{F_{CAMS}}^{int}$ (with C under the lines) respectively. Error bars in the figure show standard error of the sensitivity estimates by maximum likelihood estimates. Solid/dashed error bars indicate the estimated sensitivity from the regression approaches are statistically significant ($p < 0.05$) /insignificant ($p >= 0.05$).

by different climate forcings and land-use/land-cover changes (table S2). For the period 1981–2010, the model ensemble-mean NBP is larger than R + L, but in-between the land flux estimates from two inversion systems (table 1). Inversion estimates include anthropogenic and natural CO_2 land uptake, the latter part including the carbon cycle of aquatic continuum from land to ocean (e.g. inland waters; Regnier *et al* 2013), which can explain why their land sink is larger than the R + L. R + L only account for the overall perturbation of the global carbon cycle caused by anthropogenic activities, (i.e. anthropogenic CO_2 sink only; Le Quéré *et al* 2015). But models only estimate the anthropogenic CO_2 sink if their spin-up was correctly performed, so they should be comparable with R + L. In addition, it should be kept in mind that even though the R + L is, to our knowledge, the most comprehensive assessment of the terrestrial net carbon flux, the component RLS and E_{LUC} were reported to have an uncertainty of ± 0.8 Pg C yr^{-1} and ± 0.5 Pg C yr^{-1} respectively (Le Quéré *et al* 2015). The

insignificant correlation between global GPP and NBP across the ISIMIP2a biome models ($r = 0.34$, $p = 0.23$ across the 14 simulations considering land-use change; figure 1) indicates that larger modeled GPP does not necessarily result in larger NBP. This finding is consistent with the previous result derived from another model ensemble reported by Piao *et al* (2013). The differences in carbon residence times and/or in GPP trends may explain the differences in NBP among models. For example, we found that global NBP is significantly correlated with the trend of GPP across the 14 simulations that consider land-use change ($r = 0.39$, $p < 0.05$).

4.2. Regional contributions to the NBP interannual variation

The ISIMIP2a biome models capture the interannual variation of global net terrestrial ecosystem carbon fluxes well, given the high correlation between NBP variability and the variability in the R + L (figure 2) or the two inversion systems (table 1), where NBP driven

Table 3. The trends in NBP, NPP and Rh simulated by ISIMIP2a biome models and the ensemble-mean for the period 1990−2009.

| | PGFv2 climate forcing | | | | | |
	NBP trend (Pg C yr^{-2})	*P* value	NPP trend (Pg C yr^{-2})	*P* value	Rh trend (Pg C yr^{-2})	*P* value
CARAIB	0.035	0.397	0.174	0.000	0.137	0.000
DLEM	0.029	0.128	0.163	0.000	0.134	0.000
JULES	0.003	0.878	0.116	0.001	0.113	0.000
LPJ-GUESS	0.047	0.402	0.159	0.001	0.110	0.000
LPJmL	0.057	0.216	0.156	0.003	0.041	0.043
ORCHIDEE	0.056	0.018	0.173	0.000	0.120	0.000
VEGAS	0.051	0.063	0.106	0.003	0.042	0.021
VISIT	0.068	0.069	0.218	0.000	0.164	0.000
Ensemble[a]	**0.044**	**0.107**	**0.156**	**0.000**	**0.103**	**0.000**
SD[a]	**0.022**		**0.037**		**0.046**	
	GSWP3 climate forcing					
CARAIB	0.145	0.006	0.250	0.000	0.104	0.000
DLEM	0.033	0.137	0.166	0.000	0.133	0.000
JULES	0.041	0.192	0.186	0.002	0.145	0.000
LPJ-GUESS	0.050	0.465	0.174	0.001	0.089	0.000
LPJmL	0.095	0.062	0.190	0.001	0.041	0.047
ORCHIDEE	0.066	0.020	0.174	0.000	0.109	0.000
VEGAS	0.048	0.118	0.108	0.007	0.042	0.043
VISIT	0.087	0.087	0.233	0.000	0.150	0.000
Ensemble[a]	**0.060**	**0.091**	**0.176**	**0.000**	**0.101**	**0.000**
SD[a]	**0.024**		**0.037**		**0.046**	

[a] The ensemble-mean and SD is calculated based on the results from 7 models considering land-use change (i.e. without CARAIB).

by GSWP3 forcing shows higher correlation coefficient than that driven by PGFv2 forcing. Though tropical NBP only represents 31 ± 17% of global total NBP during the recent decades, the year-to-year variation of tropical NBP is a major contributor to the variation of global NBP (table 2), which could be seen from 1) synchronous variation between the modeled global NBP and tropical NBP ($r = 0.90 \pm 0.05$; section 3.1), and 2) the similar magnitude of variation of tropical NBP (0.9 ± 0.3 Pg C yr^{-1}) compared to variation of global NBP (1.1 ± 0.3 Pg C yr^{-1}). The major contribution of tropical NBP variation to global NBP variation in ISIMIP2a models is consistent with the earlier findings (Cox *et al* 2013, Wang *et al* 2013). The significant NPP anomalies over the SH extra-tropical regions, with the same sign as the global NPP anomalies, suggest that the SH extra-tropical ecosystems also play an important role in controlling the variation of global NPP and thus global NBP (table 2, figure S2), which is consistent with the finding of Poulter *et al* (2014). In contrast, the NPP anomalies over NH extra-tropical regions show opposite phase, which partly compensate the carbon fluxes interannual variation of other regions (table 2).

4.3. Driving factors of NBP and its trend
The simulated global carbon sink (i.e. positive NBP; over 42% of vegetated land) and its positive trend (over 18% of vegetated land) in models is partly derived from the larger global NPP increase than the Rh increase in the past decades (figure S3 and S4; also see table 3 for the period of 1990–2009; equation (2)),

suggesting that NBP in the models is more driven by the change of NPP than by the change of Rh. The environmental changes in the recent decades including elevated CO_2 concentration, climate change, nitrogen fertilization (including nitrogen deposition which only DLEM and LPJ-GUESS account for in this study), and anthropogenic land-use change have caused deviations from zero of the terrestrial carbon balance. The nonsynchronous evolution of NPP and Rh causes the positive NEP (and further increase NBP; figure 2). For the past two decades (1990–2009), the ensemble-mean trends in global NPP and Rh (driven by PGFv2 and GSWP3 climate forcings, excluding CARAIB; table 3) are lower than the trends derived from TRENDY model ensembles (NPP trend of 0.22 ± 0.08 Pg C yr^{-2} and Rh trend of 0.16 ± 0.05 Pg C yr^{-2}; S_L2 run: changing CO_2 and climate, and time-invariant present-day land use mask; Sitch *et al* 2015), which was driven by CRU-NCEP climate forcing (Viovy 2014) and did not consider land-use change in S_L2 run (Sitch *et al* 2015). The simulated NBP trend driven by GSWP3 forcing (0.060 ± 0.024 Pg C yr^{-2}) is larger than ($p = 0.05$ with paired Student's t-test) that driven by PGFv2 forcing (0.044 ± 0.022 Pg C yr^{-2}), while the NBP trend derived from TRENDY model ensembles (0.055 ± 0.030 Pg C yr^{-2}) is in-between ISIMIP2a NBPs when both forcings were considered, which implies an uncertainty of NBP trend due to uncertain trends of climate forcings, an often overlooked factor when attributing trends of carbon cycle variables to climate change (e.g. Sitch *et al* 2015). The ensemble-mean NBP trends (including ISIMIP2a and TRENDY)

are larger than the trends in R + L (0.025 Pg C yr^{-2} for 1990–2009, $p = 0.57$; Le Quéré *et al* 2015) but similar to the trends from two long-term CO_2 inversion systems: CAMS v15r2 (0.057 Pg C yr^{-2}, $p = 0.17$) and Jena CarboScope s81_v3.8 (0.052 Pg C yr^{-2}, $p = 0.16$). It is noteworthy that the ISIMIP2a and TRENDY model ensembles contain 4 common models: JULES, LPJ-GUESS, ORCHIDEE and VEGAS. Analyzing the model ensemble results from different model inter-comparison projects (e.g. ISIMIP2a and TRENDY) and/or driven by different reconstructed forcings (e.g. PGFv2 and GSWP3 climate forcings in this study) could help better understanding the forcing-induced uncertainties/ranges in carbon cycle estimation.

Despite the differences in the global ensemble-mean trends in NBP, NPP and Rh from ISIMIP2a (table 3) and TRENDY models (Sitch *et al* 2015), the spatial pattern of the trends (figure S5 and figures in Sitch *et al* 2015) is very similar. Similar spatial pattern of the positive modeled mean NBP (i.e. large mean carbon sink; figure 3(*a*)), increasing NPP (figure S4(*a*) and S3) and of the positive trend of NBP (figure 3(*b*) and S5) is found for the model ensemble-mean in many regions, such as tropical forest in northern South America, Africa and Asia, eastern Brazil, southeast Asia, south China, and the middle-to-high latitude regions in north hemisphere (also see figure S5).

The widespread increase of NPP is mainly due to the elevated CO_2 concentration (see Sitch *et al* 2015, with 4 mutual models in ISIMIP2a and TRENDY). It has the dual effect of increasing leaf photosynthesis and reducing stomatal conductance, thus increasing water-use efficiency (Rotter and Van de Geijn, 1999, Keenan *et al* 2013). A CO_2 fertilization effect on photosynthesis for C3 (Farquhar *et al* 1980) and C4 species (Collatz *et al* 1992) is included in all ISIMIP2a biome models. The magnitude of these effects is, however, heavily debated, for example as population dynamics, which are not represented in great detail in all ISIMIP2a models, might undo physiological effects at the stand scale (e.g. Hickler *et al* 2015). For temperate and high-latitude (cold) ecosystems in northern hemisphere (figure S4(*a*)), NPP could be further enhanced through gradually growing season extension due to the warming trend (e.g. Myneni *et al* 1997, Tucker *et al* 2001, Piao *et al* 2007). In addition, nitrogen fertilization (including nitrogen deposition) may enhance vegetation productivity in the models accounting for nitrogen interactions (i.e. DLEM and LPJ-GUESS in this study). The goal of ISIMIP2a was not to separate the impact of these factors, while their effects could be revealed through other studies with common models regarding NPP-related variables such as LAI (Zhu *et al* 2016) and evapotranspiration (Mao *et al* 2015).

A carbon sink is also simulated by a majority of simulations in the Amazon basin and eastern Australia, where NPP is higher than Rh (thus results in positive NBP; data not shown), despite a near-zero or negative NPP trend simulated in some areas (e.g. south Amazon basin, and eastern Australia; figure S4 (*a*)). However, this carbon sink became weaker in the recent decades (negative NBP trend; figure 3(*b*)), possibly and partly due to a combination of climate and land-use change in these regions. For example, 13 out of 14 simulations considering land-use change showed a negative NBP trend over intact forest in the Amazon basins (with decreasing rate of -0.50 ± 0.54 gC m^{-2}yr^{-2} and -1.08 ± 0.56 gC m^{-2}yr^{-2} driven by PGFv2 and GSWP3 forcing respectively), due to the larger increase in Rh than in NPP. Here, intact forest was defined as the grid cells with less than 2% changes in the agricultural fraction of land. In regions that experienced significant agricultural expansion over Amazon basin (i.e. grid cells with more than 2% increase in agricultural fraction during 1971–2010), all simulations showed a negative NBP trend (with decreasing rate of -0.76 ± 0.42 gC m^{-2}yr^{-2} and -1.00 ± 0.55 gC m^{-2}yr^{-2} driven by PGFv2 and GSWP3 forcing respectively), which could be a result of increased Rh due to deforestation and smaller increase in NPP, or even decreased NPP in 5 out of 14 simulations.

Anthropogenic land-use change is another important factor causing the positive or negative NBP simulated by model ensembles (figure 3(*a*)). Deforestation for agriculture through wood harvest or burning due to fire could cause intensive carbon loss in reality (e.g. South America, Sub-Saharan Africa, and Southeast Asia in figure 3, figure S6, and table S3; Guo and Gifford 2002, Van der Werf *et al* 2009), but the fate of carbon after forest loss is represented differently in the biome models where harvested biomass can go either into litter pools (increase Rh; all models), product pools (DLEM) or directly to the atmosphere through burning (DLEM). In addition, a carbon source can be sustained by the removal of above-ground biomass by agricultural practices such as harvest (i.e. positive $C_{harvest}$ in equation (1)). In contrast to the agriculture expansion over tropical regions, there are land-use changes characterized by the abandonment of the agricultural land and possible reforestation in eastern United States (table S3), Europe, eastern Russia and eastern China (figure S6). The abandonment of the agricultural land eliminates the carbon export as agricultural products, increasing the carbon input into soil, and may increase biomass carbon stock by aforestation. All of these processes could induce positive NBP in these regions (figure 3 and S2).

4.4. Biome model response to ENSO events
A stronger global carbon sink during the La Niña years than that during the El Niño years is found for the R + L estimate, and is also simulated by all biome models in this study, implying consistent model capability in capturing the net terrestrial carbon fluxes deviation

between the two phases of ENSO at global scale. Model simulations reveal that the NBP deviation during ENSO events could be mainly attributed to the NPP deviation. Rh deviation partly offsets the NPP deviation in 6 out of 8 models (range from 13% for LPJmL to 52% for JULES), CARAIB and LPJ-GUESS being exceptions. ΔRh_{L-E} is negative for CARAIB (i.e. enhance the NBP deviation), and marginal for LPJ-GUESS. This suggests that the climate anomalies during ENSO events cause the same direction of deviation on NPP and Rh, though that may not always be the case. The very similar spatial pattern between NBP and NPP anomalies during ENSO events confirms again that the NBP deviation is mainly due to the NPP deviation in the biome models. Furthermore, the NDVI anomalies during ENSO events agree in the sign of the modeled NPP anomalies for most regions, globally (section 3.2; figure 5), suggesting that the ISIMIP2a biome models generally are able to capture the NPP anomaly during ENSO events. In the lower part of the Amazon basin and tropical forest in Africa, the opposite sign of anomalies found between modeled NPP and NDVI during the La Niña years could be the result of poor climate data input based on few stations. Apart from the NPP induced NBP deviation during ENSO events, anomalies of fire emissions could also contribute to the NBP deviation. For example, the tropical fire emission anomaly caused by strong 1997–1998 El Niño events was estimated to have a significant contribution to the net terrestrial carbon fluxes anomaly and thus the CO_2 growth rate in that period (Page *et al* 2002, van der Werf *et al* 2004, Betts *et al* 2016).

During El Niño years, ISIMIP2a models simulate negative NPP anomalies (lower NPP) over eastern and northern Canada and western Siberia (dominantly boreal ecosystems), but positive NPP anomaly for these regions during the La Niña years, which could be primarily due to the temperature anomalies. Higher mean annual temperature during the La Niña years (figure 5(*d*) and S3(*b*)) has the potential to extend the growing season in these regions, possibly partly through advancing the snow-melt (Kirdyanov *et al* 2003, Piao *et al* 2007) and enhanced photosynthesis, and with the opposite effect during El Niño years (figure 5(c) and S3(a)). It is noteworthy that the impacts could be diverse for different types of El Niño events (e.g. Capotondi *et al* 2015), which were not analyzed separately in this study.

For tropical and sub-tropical regions, the positive NPP anomaly generally coincides with a positive precipitation anomaly and a negative temperature anomaly, and vice versa (figures 5(*c*) and (*d*), S7(*a*)−(*d*)). Higher temperature plus lower precipitation increase water deficit (possibly causing drought) over tropical and sub-tropical regions, which tends to reduce productivity in savannas (a water-limit ecosystem) and forests (Tribuzy 2005, Doughty and Goulden 2008), and increase tree mortality in tropical forest (Allen *et al* 2010, Phillips

et al 2010). Conversely, tropical vegetation generally prospers in the years with lower temperature (negative anomaly) and higher precipitation (positive anomaly; figures S7(*b*) and (*d*)), where higher NPP is simulated by models (figures 5(*c*) and (*d*)). The ΔNBP_{L-E} and ΔNPP_{L-E} over tropical regions (23°S–23°N) dominate the global anomaly differences between ENSO events (section 3.2; figures 4(*a*) and (*b*)), which again implies that the interannual variation of global NBP is mainly caused by the tropical NBP variation in models. Furthermore, considering the tight coincidence between tropical NBP anomalies and tropical climate anomalies, the global terrestrial carbon flux anomalies may be strongly driven by the tropical climate anomalies.

4.5. Biome model response to tropical climate
The ISIMIP2a biome models responses to tropical climate are generally consistent with the earlier findings (e.g. Baker *et al* 2006, Cox *et al* 2013, Wang *et al* 2013, Wang *et al* 2014), which suggest that year-to-year variations in global carbon fluxes are strongly connected with the tropical climate variation. Tropical solar radiation variation does not significantly impact the global net carbon fluxes variation, given the fact that φ^{int}_{NBP}, φ^{int}_{R+L}, $\varphi^{int}_{F_{Jena}}$ and $\varphi^{int}_{F_{CAMS}}$ are all not significant statistically. However, the different responses to tropical temperature and precipitation derived from modeled NBP and R + L and inversions (section 3.3) suggest that some models may be under-sensitive to tropical temperature variations, but over-sensitive to tropical precipitation variations for their simulated net terrestrial carbon fluxes (i.e. NBP), which is consistent with the findings from TRENDY models (Piao *et al* 2013). It should be noted that the sensitivities obtained in this study only indicates the response of the global spatially averaged carbon fluxes interannual variability to the climate variability averaged for tropical region. The regional (or local) carbon fluxes interannual variability could have different sensitivities to the local climate variability (e.g. stronger response to precipitation and/or radiation variations). For example, Ahlstrom *et al* (2015) found that global NBP interannual variability becomes more correlated with precipitation (almost as strong as correlation with temperature) at higher levels of disaggregation of climate variables. There is significant correlation between and γ^{int}_{NBP} and $\delta^{int}_{NBP}(r = 0.71, p < 0.05)$ across the model ensemble, which means that high (or low) sensitivity to tropical temperatures may compensate for low (or high) sensitivity to tropical precipitations (i.e. with sensitivity compensation). Furthermore, high positive correlation between δ^{int}_{NBP} and $\delta^{int}_{GPP}(r = 0.80, p < 0.05)$, and between δ^{int}_{NBP} and $\delta^{int}_{Rh}(r = 0.65, p < 0.08)$ between across model ensemble suggests that the model differences in global NBP response to tropical precipitation variation depend on both NPP and Rh.

5. Concluding remarks

In this study, we evaluate the NBP from the eight ISIMIP2a biome models against the net global terrestrial ecosystem carbon fluxes that include the land-use-change emissions (E_{LUC}) and the 'residual' land sink (RLS) derived from the GCP carbon budget analysis by Le Quéré *et al* (2015) for the period of 1971–2010. We focus on the mean value, spatial distribution, trend and interannual variability of NBP, and investigate the carbon fluxes deviation due to ENSO events. A special attention is paid to the sensitivity of global NBP to tropical climate variability. We found that:

1. the ensemble-mean annual NBP (sink) is higher than but within the uncertainty of R + L, while simulated NBP trends are lower than that from R + L; models capture the interannual variability of NBP well;

2. tropical NBP represents 31 ± 17% of global total NBP during the past decades, and the year-to-year variation of tropical NBP is the major contributor to variation of global NBP.

3. different ensemble-mean NBP trends when driven by different climate forcings implies a significant uncertainty of NBP trend due to uncertain trends of climate forcings, an often overlooked factor when attributing trends of carbon cycle variables to climate.

4. all models simulate significant global NBP deviation between El Niño and La Niña years and mainly due to NPP deviation. NDVI shows similar, but not as distinct as significant, deviation between El Niño and La Niña years.

5. the different global net land carbon flux sensitivities to tropical temperature and precipitation derived from modeled NBP, R + L and inversions indicate that some models may be under-sensitive to tropical temperature variation, but over-sensitive to tropical precipitation variation for their simulated NBP.

Acknowledgments

References

Ahlström A *et al* 2015 The dominant role of semi-arid ecosystems in the trend and variability of the land CO_2 sink *Science* **348** 895–9

Alden C B, Miller J B and White J W 2010 Can bottom-up ocean CO_2 fluxes be reconciled with atmospheric 13C observations? *Tellus* B **62** 369–88

Allen C D, Macalady A K, Chenchouni H, Bachelet D, McDowell N, Vennetier M, Kitzberger T, Rigling A, Breshears D D, and Hogg E T 2010 A global overview of drought and heat-induced tree mortality reveals emerging climate change risks for forests *For. Ecol. Manage.* **259** 660–84

Baker D, Law R M, Gurney K, Rayner P, Peylin P, Denning A, Bousquet P, Bruhwiler L, Chen Y H and Ciais P 2006 TransCom 3 inversion intercomparison: impact of transport model errors on the interannual variability of regional CO_2 fluxes, 1988–2003 *Glob. Biogeochem. Cycles* **20** GB1002

Best M, Pryor M, Clark D, Rooney G, Essery R, Ménard C, Edwards J, Hendry M, Porson A and Gedney N 2011 The joint UK land environment simulator (JULES), model description—part 1: energy and water fluxes *Geosci. Model Dev.* **4** 677–99

Betts R A, Jones C D, Knight J R, Keeling R F and Kennedy J J 2016 El Nino and a record CO_2 rise *Nat. Clim. Change* **6** 806–10

Bondeau A, Smith P C, Zaehle S, Schaphoff S, Lucht W, Cramer W, Gerten D, Lotze-campen H, Müller C and Reichstein M 2007 Modelling the role of agriculture for the 20th century global terrestrial carbon balance *Glob. Change Biol.* **13** 679–706

Capotondi A, Wittenberg A T, Newman M, Di Lorenzo E, Yu J-Y, Braconnot P, Cole J, Dewitte B, Giese B and Guilyardi E 2015 Understanding ENSO diversity *Bull. Am. Meteorol. Soc.* **96** 921–38

Chevallier F 2013 On the parallelization of atmospheric inversions of CO_2 surface fluxes within a variational framework *Geosci. Model Dev.* **6** 783–90

Chevallier F, Ciais P, Conway T, Aalto T, Anderson B, Bousquet P, Brunke E, Ciattaglia L, Esaki Y and Fröhlich M 2010 CO_2 surface fluxes at grid point scale estimated from a global 21 year reanalysis of atmospheric measurements *J. Geophys. Res. Atmos.* **115** D21307

Chevallier F, Fisher M, Peylin P, Serrar S, Bousquet P, Bréon F M, Chédin A and Ciais P 2005 Inferring CO_2 sources and sinks from satellite observations: method and application to TOVS data *J. Geophys. Res. Atmos.* **110** D24309

Ciais P, Reichstein M, Viovy N, Granier A, Ogée J, Allard V, Aubinet M, Buchmann N, Bernhofer C and Carrara A 2005 Europe-wide reduction in primary productivity caused by the heat and drought in 2003 *Nature* **437** 529–33

Clark D, Mercado L, Sitch S, Jones C, Gedney N, Best M, Pryor M, Rooney G, Essery R and Blyth E 2011 The joint UK land environment simulator (JULES), model description−part 2: carbon fluxes and vegetation dynamics *Geosci. Model Dev.* **4** 701–22

Cleveland C C, Townsend A R, Schimel D S, Fisher H, Howarth R W, Hedin L O, Perakis S S, Latty E F, Von Fischer J C and Elseroad A 1999 Global patterns of terrestrial biological nitrogen (N_2) fixation in natural ecosystems *Glob. Biogeochem. Cycles* **13** 623–45

Collatz G J, Ribas-Carbo M and Berry J 1992 Coupled photosynthesis-stomatal conductance model for leaves of C4 plants *Funct. Plant Biol.* **19** 519–38

Cox P M, Pearson D, Booth B B, Friedlingstein P, Huntingford C, Jones C D and Luke C M 2013 Sensitivity of tropical carbon to climate change constrained by carbon dioxide variability *Nature* **494** 341–4

Cramer W, Bondeau A, Woodward F I, Prentice I C, Betts R A, Brovkin V, Cox P M, Fisher V, Foley J A and Friend A D 2001 Global response of terrestrial ecosystem structure and function to CO_2 and climate change: results from six dynamic global vegetation models *Glob. Change Biol.* **7** 357–73

Dawson A and O'Hare G 2000 Ocean-atmosphere circulation and global climate: the El-Niño-Southern oscillation *Geogr. J. Geogr. Assoc.* **85** 193

Doughty C E and Goulden M L 2008 Are tropical forests near a high temperature threshold *J. Geophys. Res. Biogeosci.* **113** G00B07

Dury M, Hambuckers A, Warnant P, Henrot A, Favre E, Ouberdous M and François L 2011 Responses of European forest ecosystems to 21st century climate: assessing changes in interannual variability and fire intensity *iForest-Biogeosciences and Forestry* **4** 82

Farquhar G V, von Caemmerer S V and Berry J 1980 A biochemical model of photosynthetic CO_2 assimilation in leaves of C3 species *Planta* **149** 78–90

Frank D, Reichstein M, Bahn M, Thonicke K, Frank D, Mahecha M D, Smith P, Velde M, Vicca S and Babst F 2015 Effects of climate extremes on the terrestrial carbon cycle: concepts, processes and potential future impacts *Glob. Change Biol.* **21** 2861–80

Friedlingstein P, Cox P, Betts R, Bopp L, Von Bloh W, Brovkin V, Cadule P, Doney S, Eby M and Fung I 2006 Climate-carbon cycle feedback analysis: results from the C4MIP model intercomparison *J. Clim.* **19** 3337–53

Gatti L, Gloor M, Miller J, Doughty C, Malhi Y, Domingues L, Basso L, Martinewski A, Correia C and Borges V 2014 Drought sensitivity of Amazonian carbon balance revealed by atmospheric measurements *Nature* **506** 76–80

Guo L B and Gifford R 2002 Soil carbon stocks and land use change: a meta analysis *Glob. Change Biol.* **8** 345–60

Gérard J-C, Nemry B, Francois L and Warnant P 1999 The interannual change of atmospheric CO_2: contribution of subtropical ecosystems? *Geophys. Res. Lett.* **26** 243–6

Hickler T, Rammig A and Werner C 2015 Modelling CO_2 impacts on forest productivity *Curr. Forest. Rep.* **1** 69–80

Huntzinger D, Schwalm C, Michalak A, Cook R, Jacobson A, Schaefer K, Dasgupta A and Poco J 2013 Global net land carbon sink: results from the Multi-scale Synthesis and Terrestrial Model Intercomparison Project (MsTMIP) *AGU Fall Meeting Abstracts*

Huntzinger D N, Schwalm C, Michalak A, Schaefer K, King A, Wei Y, Jacobson A, Liu S, Cook R and Post W 2013 The north american carbon program multi-scale synthesis and terrestrial model intercomparison project—part 1: overview and experimental design *Geosci. Model Dev.* **6** 2121–33

Ito A and Inatomi M 2012 Water-use efficiency of the terrestrial biosphere: a model analysis focusing on interactions between the global carbon and water cycles *J. Hydrometeorol.* **13** 681–94

Keeling C D and Whorf T P 2005 Atmospheric CO_2 records from sites in the SIO sampling network *Trends: A Compendium of Data on Global Change* (Oak Ridge, TN, USA: Carbon Dioxide Information Analysis Center, Oak Ridge National Laboratory, U.S. Department of Energy) (http://cdiac.ornl.gov/trends/co2/sio-mlo.htm)

Keenan T F, Hollinger D Y, Bohrer G, Dragoni D, Munger J W, Schmid H P and Richardson A D 2013 Increase in forest water-use efficiency as atmospheric carbon dioxide concentrations rise *Nature* **499** 324–7

Kirdyanov A, Hughes M, Vaganov E, Schweingruber F and Silkin P 2003 The importance of early summer temperature and date of snow melt for tree growth in the Siberian subarctic *Trees* **17** 61–9

Krinner G, Viovy N, de Noblet-Ducoudré N, Ogée J, Polcher J, Friedlingstein P, Ciais P, Sitch S and Prentice I C 2005 A dynamic global vegetation model for studies of the coupled atmosphere-biosphere system *Glob. Biogeochem. Cycles* **19** GB1015

Lamarque J-F, Dentener F, McConnell J, Ro C-U, Shaw M, Vet R, Bergmann D, Cameron-Smith P, Doherty R and Faluvegi G 2013 Multi-model mean nitrogen and sulfur deposition from the Atmospheric Chemistry and Climate Model Intercomparison Project (ACCMIP): evaluation historical and projected changes

Lamarque J-F, Kyle G P, Meinshausen M, Riahi K, Smith S J, van Vuuren D P, Conley A J and Vitt F 2011 Global and regional evolution of short-lived radiatively-active gases and aerosols in the Representative Concentration Pathways *Clim. Change* **109** 191–212

Le Quéré C, Moriarty R, Andrew R M, Canadell J G, Sitch S, Korsbakken J I, Friedlingstein P, Peters G P, Andres R J and Boden T 2015 Global carbon budget 2015 *Earth Syst. Sci. Data* **7** 349–96

Lee K, Wanninkhof R, Takahashi T, Doney S C and Feely R A 1998 Low interannual variability in recent oceanic uptake of atmospheric carbon dioxide *Nature* **396** 155–9

Lu C and Tian H 2017 Global nitrogen and phosphorus fertilizer use for agriculture production in the past half century: shifted hot spots and nutrient imbalance *Earth Syst. Sci. Data* **9** 181–92

Mao J, Fu W, Shi X, Ricciuto D M, Fisher J B, Dickinson R E, Wei Y, Shem W, Piao S and Wang K 2015 Disentangling climatic and anthropogenic controls on global terrestrial evapotranspiration trends *Environ. Res. Lett.* **10** 094008

Mitchell T D and Jones P D 2005 An improved method of constructing a database of monthly climate observations and associated high-resolution grids *Int. J. Climatol.* **25** 693–712

Myneni R B, Keeling C D, Tucker C J, Asrar G and Nemani R R 1997 Increased plant growth in the northern high latitudes from 1981 to 1991 *Nature* **386** 698–702

Page S E, Siegert F, Rieley J O, Boehm H-D V, Jaya A and Limin S 2002 The amount of carbon released from peat and forest fires in Indonesia during 1997 *Nature* **420** 61–5

Pan Y, Birdsey R A, Fang J, Houghton R, Kauppi P E, Kurz W A, Phillips O L, Shvidenko A, Lewis S L and Canadell J G 2011 A large and persistent carbon sink in the world's forests *Science* **333** 988–93

Phillips O L, Van Der Heijden G, Lewis S L, López-González G, Aragão L E, Lloyd J, Malhi Y, Monteagudo A, Almeida S and Dávila E A 2010 Drought—mortality relationships for tropical forests *New Phytol.* **187** 631–46

Piao S, Friedlingstein P, Ciais P Viovy N and Demarty J 2007 Growing season extension and its impact on terrestrial carbon cycle in the Northern Hemisphere over the past 2 decades *Glob. Biogeochem. Cycles* **21** GB3018

Piao S, Sitch S, Ciais P, Friedlingstein P, Peylin P, Wang X, Ahlström A, Anav A, Canadell J G and Cong N 2013 Evaluation of terrestrial carbon cycle models for their response to climate variability and to CO_2 trends *Glob. Change Biol.* **19** 2117–32

Poulter B, Frank D, Ciais P, Myneni R B, Andela N, Bi J, Broquet G, Canadell J G, Chevallier F and Liu Y Y 2014 Contribution of semi-arid ecosystems to interannual variability of the global carbon cycle *Nature* **509** 600–3

Regnier P, Friedlingstein P, Ciais P, Mackenzie F T, Gruber N, Janssens I A, Laruelle G G, Lauerwald R, Luyssaert S and Andersson A J 2013 Anthropogenic perturbation of the carbon fluxes from land to ocean *Nat. Geosci.* **6** 597–607

Reichstein M, Bahn M, Ciais P, Frank D, Mahecha M D, Seneviratne S I, Zscheischler J, Beer C, Buchmann N and Frank D C 2013 Climate extremes and the carbon cycle *Nature* **500** 287–95

Robock A 2000 Volcanic eruptions and climate *Rev. Geophys.* **38** 191–219

Rödenbeck C, Conway T and Langenfelds R 2006 The effect of systematic measurement errors on atmospheric CO_2 inversions: a quantitative assessment *Atmos. Chem. Phys.* **6** 149–61

Rödenbeck C, Houweling S, Gloor M and Heimann M 2003 CO_2 flux history 1982–2001 inferred from atmospheric data using a global inversion of atmospheric transport *Atmos. Chem. Phys.* **3** 1919–64

Rötter R and Van de Geijn S 1999 Climate change effects on plant growth, crop yield and livestock *Clim. Change* **43** 651–81

Sitch S, Friedlingstein P, Gruber N, Jones S, Murray-Tortarolo G, Ahlström A, Doney S C, Graven H, Heinze C and Huntingford C 2015 Recent trends and drivers of regional sources and sinks of carbon dioxide *Biogeosciences* **12** 653–79

Sitch S, Huntingford C, Gedney N, Levy P, Lomas M, Piao S, Betts R, Ciais P, Cox P and Friedlingstein P 2008 Evaluation of the terrestrial carbon cycle, future plant geography and climate-carbon cycle feedbacks using five Dynamic Global Vegetation Models (DGVMs) *Glob. Change Biol.* **14** 2015–39

Smith B, Warlind D, Arneth A, Hickler T, Leadley P, Siltberg J and Zaehle S 2014 Implications of incorporating N cycling and N limitations on primary production in an individual-based dynamic vegetation model *Biogeosciences* **11** 2027–54

Smith W K, Reed S C, Cleveland C C, Ballantyne A P, Anderegg W R, Wieder W R, Liu Y Y and Running S W 2016 Large divergence of satellite and earth system model estimates of global terrestrial CO_2 fertilization *Nat. Clim. Change* **6** 306–10

Stocker B D, Feissli F, Strassmann K M, Spahni R and Joos F 2014 Past and future carbon fluxes from land use change, shifting cultivation and wood harvest *Tellus* B **66** 23118

Tian H, Chen G, Lu C, Xu X, Hayes D J, Ren W, Pan S, Huntzinger D N and Wofsy S C 2015a North American terrestrial CO_2 uptake largely offset by CH_4 and N_2O emissions: toward a full accounting of the greenhouse gas budget *Clim. Change* **129** 413–6

Tian H, Chen G, Lu C, Xu X, Ren W, Zhang B, Banger K, Tao B, Pan S and Liu M 2015b Global methane and nitrous oxide emissions from terrestrial ecosystems due to multiple environmental changes *Ecosyst. Health Sustainability* **1** 1–20

Tribuzy E S 2005 Variações da temperatura foliar do dossel e o seu efeito na taxa assimilatória de CO_2 na Amazônia Central, Universidade de São Paulo

Tucker C J, Pinzon J E, Brown M E, Slayback D A, Pak E W, Mahoney R, Vermote E F and El Saleous N 2005 An extended AVHRR 8-km NDVI dataset compatible with MODIS and SPOT vegetation NDVI data *Int. J. Remote Sens.* **26** 4485–98

Tucker C J, Slayback D A, Pinzon J E, Los S O, Myneni R B and Taylor M G 2001 Higher northern latitude normalized difference vegetation index and growing season trends from 1982 to 1999 *Int. J. Biometeorol.* **45** 184–90

Van der Werf G R, Morton D C, DeFries R S, Olivier J G, Kasibhatla P S, Jackson R B, Collatz G J and Randerson J T 2009 CO_2 emissions from forest loss *Nat. Geosci.* **2** 737–8

Van Der Werf G R, Randerson J T, Collatz G J, Giglio L, Kasibhatla P S, Arellano A F, Olsen S C and Kasischke E S 2004 Continental-scale partitioning of fire emissions during the 1997 to 2001 El Nino/La nina period *Science* **303** 73–6

Viovy N 2014 CRU-NCEPv4. CRUNCEP dataset (http://dods. extra.cea.fr/data/p529viov/cruncep/readme.htm)

Wang W, Ciais P, Nemani R R, Canadell J G, Piao S, Sitch S, White M A, Hashimoto H, Milesi C and Myneni R B 2013 Variations in atmospheric CO_2 growth rates coupled with tropical temperature *Proc. Natl Acad. Sci.* **110** 13061–6

Wang X, Piao S, Ciais P, Friedlingstein P, Myneni R B, Cox P, Heimann M, Miller J, Peng S and Wang T 2014 A two-fold increase of carbon cycle sensitivity to tropical temperature variations *Nature* **506** 212–5

Warnant P, François L, Strivay D and Gérard J C 1994 CARAIB: a global model of terrestrial biological productivity *Glob. Biogeochem. Cycles* **8** 255–70

Wei Y, Liu S, Huntzinger D N, Michalak A, Viovy N, Post W, Schwalm C R, Schaefer K, Jacobson A and Lu C 2014 The North American carbon program multi-scale synthesis and terrestrial model intercomparison project—part 2: environmental driver data *Geosci. Model Dev.* **7** 2875–93

Wolf S, Keenan T F, Fisher J B, Baldocchi D D, Desai A R, Richardson A D, Scott R L, Law B E, Litvak M E and Brunsell N A 2016 Warm spring reduced carbon cycle impact of the 2012 U.S. summer drought *Proc. Natl Acad. Sci.* **113** 5880–5

Wolter K and Timlin M S 2011 El Niño/Southern oscillation behaviour since 1871 as diagnosed in an extended multivariate ENSO index (MEI. ext) *Int. J. Climatol.* **31** 1074–87

Zeng N, Mariotti A and Wetzel P 2005 Terrestrial mechanisms of interannual CO_2 variability *Glob. Biogeochem. Cycles* **19** GB1016

Zhu Z, Piao S, Myneni R B, Huang M, Zeng Z, Canadell J G, Ciais P, Sitch S, Friedlingstein P and Arneth A 2016 Greening of the earth and its drivers *Nat. Clim. Change* **6** 791–5

Zscheischler J, Mahecha M D, von Buttlar J, Harmeling S, Jung M, Rammig A, Randerson J T, Schölkopf B, Seneviratne S I and Tomelleri E 2014a A few extreme events dominate global interannual variability in gross primary production *Environ. Res. Lett.* **9** 035001

Zscheischler J, Reichstein M, Harmeling S, Rammig A, Tomelleri E and Mahecha M D 2014b Extreme events in gross primary production: a characterization across continents *Biogeosciences* **11** 2909–24